



# A study on the effect of the die transverse angle and the part rotational feed angle in the cold radial forging process of rods

M. Fattahpoor Roushan, H. Afrasiab\*, and R.A. Jafari Talookolaei

*Department of Mechanical Engineering, Babol Noshirvani University of Technology, Babol, Iran.*

Received 9 December 2021; received in revised form 30 October 2022; accepted 16 April 2023

## KEYWORDS

Radial forging process;  
 Die transverse angle;  
 Part rotational feed angle;  
 Residual stress;  
 Product quality.

**Abstract.** Radial forging is an efficient and high-precision process for manufacturing rotary parts such as shafts, axles, and gun barrels. While this process has been extensively investigated in the literature, the effect of some parameters like the die transverse angle and the part rotational feed angle has not been adequately studied since simulating several steps of this process with a full three-dimensional model is required for this purpose, which is labor-intensive and time-consuming. To bridge this gap a three-dimensional nonlinear finite element model has been developed in this paper to analyze the effects of the die transverse angle and part rotational feed angle in this process. To address the lack of reliable experimental data in the literature, an innovative approach has been proposed and used for validation of the developed finite element model. It has been observed that dies with transverse angles of  $155^\circ$  and  $165^\circ$  provide the best performance in producing a part geometry close to the desired shape. However, the most uniform residual stress distribution is obtained in forging by a die with a smaller transverse angle. Furthermore, to improve the shape and quality of the final product, the part rotational feed angle should be reduced as much as possible.

© 2024 Sharif University of Technology. All rights reserved.

## 1. Introduction

Radial forging is an open-die forging process used for reducing the diameter of shafts, tubes, and axles and for creating internal profiles for tubes, such as rifling the gun barrels [1]. The advantages of the radial forging process lie in its capability to produce superior mechanical properties in the product, tight dimensional

and geometrical tolerances, good surface finish, high production rate, and material saving [2].

Normally, in radial forging, four hammer dies are radially arranged around the part. The part is shaped by the impact of dies moving reciprocally with short course and high frequency. The part displacement in the radial forging process consists of both translational and rotational motions [3]. The translational component is performed to feed the part through the dies, and the rotational motion is used to achieve a round, circular shape. Both of these motions are

\*. Corresponding author. Tel.: +98 11 35501321;  
 Fax: +98 11 32334201  
 E-mail address: [afrasiab@nit.ac.ir](mailto:afrasiab@nit.ac.ir) (H. Afrasiab)

### To cite this article:

M. Fattahpoor Roushan, H. Afrasiab, and R. Jafari Talookolaei "A study on the effect of the die transverse angle and the part rotational feed angle in the cold radial forging process of rods", *Scientia Iranica* (2024), 31(8), pp. 646-658

DOI: 10.24200/sci.2023.59533.6295

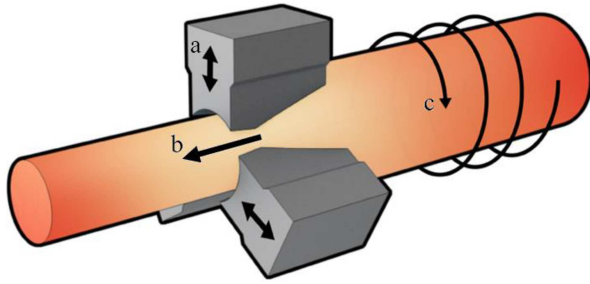


**Figure 1.** Motions in radial forging: (a) dies reciprocal movement, (b) part translation, and (c) part rotation (rotational feed).

stopped during die-part contact to prevent the part from twisting. Three principal movements of the part and dies are depicted in Figure 1.

A longitudinal cut of the radial forging die is shown in Figure 2(a). Angle  $\alpha$  in this figure is the die inlet angle. The front view of the die is presented in Figure 2(b). The die may have a curved or a bilinear lateral profile, as can be seen in this figure. In a die with a bilinear profile, the angle  $\beta$  between the lines is called the transverse angle.

Different parameters affect the outcome of the radial forging process. The radius reduction ratio, the die geometry, and the part rotational and axial feeds are among these parameters. On the other hand, different operational characteristics, such as the forming force [4], uniformity of the strain distribution [5], Residual Stresses (RSs) [6], and tool life [1], are usually investigated in the literature to evaluate the performance of this process. Among these operational characteristics, the strain and RS distributions are of particular importance due to their effect on the dimensional stability, mechanical properties, and operational life of the process product [7].

The radial forging process has been generally studied by one of the analytical or Finite Element Method (FEM) approaches in the literature. Among the most popular analytical approaches, the slab method [2,7], the upper-bound method [8], and most recently the asymptotic analysis can be mentioned. For instance, Afrasiab [9] conducted an improved upper-bound analysis to predict the void closure behavior

in the metal billets. In another study, Afrasiab et al. [10] proposed an analytical approach based on the asymptotic analysis to develop an axisymmetric model for the radial forging process of rods. While analytical approaches can provide a fast means to obtain the solution, none of them are as accurate and powerful as the FEM. Subsequently, many articles have employed this method for studying different aspects of the radial forging process. For instance, Afrasiab and Movahhedy [1] studied the effect of different parameters on the tooling life by a 3D FEM. In [7], Afrasiab used the 3D FEM for improving the die design in the radial forging of tubes without a mandrel. Darki and Raskatov [11] conducted a symmetric 3D finite element simulation to obtain the contours of RS, strain velocity, and temperature and to explore the influence of friction parameters on the contact force, stresses, and equivalent strains. Wang and Dong [12] developed a FEM to study the influence of the Lode parameter on the void evolution behavior of the power-law viscous solids in the radial forging process. Yang et al. [13] focused on the effect of cold radial forging on the forged steel tube under different forging reductions. Xu et al. [14] investigated the evolution of the RS during the annealing of steel tubes processed by cold radial forging. Zuev et al. [15] examined the effect of radial forging on the mechanical properties of Ti-based alloys. Zou et al. [16] studied the deformation mechanism of ZK60 magnesium bars during radial forging. The microstructural and mechanical response of ZK60 magnesium alloy subjected to radial forging was considered by Zou et al. [17] in another study. Yang et al. [18] employed a two-dimensional polycrystalline FEM to simulate the microstructure and the texture of the 30SiMn2MoVA steel gun barrel processed by radial forging. Makiyama [19] conducted a finite element simulation using commercial software FORGE to study the effect of rotational feed emulating four-die radial forging on the forged shape in the mandrel-less incremental forging of a thick circular tube. Darki and Raskatov [20] developed a 3D visco-elastoplastic FEM to predict the effect of the die angle on the forging load and the RSs in the workpiece. Mackey et al. [21] used a FEM of the radial forging process with cohesive zones

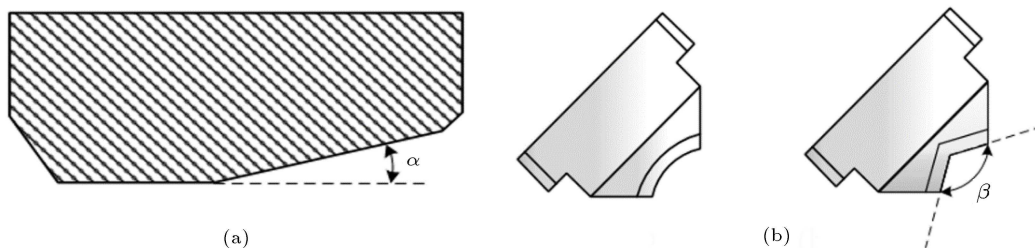


**Figure 2.** (a) Longitudinal cut of the die with the inlet angle definition; (b) Front view of the die with the transverse angle definition.

to simulate the evolution of non-metallic inclusions during the forging process.

Despite many studies performed previously on the radial forging process, some aspects of the process still need further attention. For example, an overview of the related literature shows that while the effect of parameters such as the die inlet angle, its land length, the axial feed, and the friction conditions have been extensively investigated in the literature, a comprehensive study on the effect of important parameters such as the die transverse angle or the part rotational feed has never been performed. Furthermore, in most previous studies, even the most recent ones, the effect of the rotational feed is neglected, and the variation of the die shape in the cross-section is ignored [10,13]. This is due to the fact that a full 3D model of the process is required for including these parameters in the analysis. Such a model is more complex to develop and consumes more computational time and resources. Considering this fact, a nonlinear 3D FEM of the radial forging process is developed and used in this paper to study the effect of the die transverse angle and part rotational feed on the plastic equivalent strain and RS distribution in the part. These parameters are among the most important factors affecting the final product quality. Since reliable and accurate experimental data for the radial forging process are not presented in the existing literature, an innovative experimental procedure based on two simple compression tests has been designed and implemented to verify the developed FEM.

Based on the above discussion, the main novelties of the current study are:

1. Development of a nonlinear 3D FEM for the study of the effect of the die transverse angle and part rotational feed in the radial forging process for the first time;
2. Introducing a new simple and innovative experimental method for verifying the theoretical models of the radial forging process.

A detailed description of the procedures is given in the following sections.

## 2. Methods

### 2.1. Finite Element Model (FEM)

In order to study the radial forging process, a nonlinear 3D FEM is developed in the framework of ABAQUS/Explicit commercial software. The formulation governing this model, after linearization, can be written as:

$$[M^e] \{\ddot{U}^e\} + [K^e] \{U^e\} = \{F^e\}, \quad (1)$$

where,  $[M^e]$  and  $[K^e]$  are the mass and stiffness matrices, respectively,  $\{F^e\}$  denotes the mechanical

force vector, and  $\{U^e\}$  and  $\{\ddot{U}^e\}$  are the displacement and acceleration vectors, respectively.

It is known that any element that locks volumetrically, like first-order brick elements (C3D8), will not perform well for von Mises plastic materials, which are nearly incompressible. Reduced integration is generally used to eliminate volumetric locking, which is common in modeling incompressible or nearly incompressible materials. Consequently, in this paper, first-order brick elements with reduced integration (C3D8R) are used to mesh the part (modeled as von Mises elastic-plastic material) to avoid numerical problems associated with volumetric locking, such as divergent or less accurate solutions. Since dies deformation is negligible, they are assumed to be rigid bodies in the FEM and are meshed by rigid first-order brick elements. The meshed assembly of the part and dies is shown in Figure 3.

The process can be assumed as isothermal since the process is performed at room temperature, and the heat generated during the plastic forming of the part dissipates due to heat exchange with surroundings and dies. A compression test was conducted on a sample made from the part material, which is ST37 steel. The stress-strain curve shown in Figure 4(a) was obtained in this test. The raw data related to this compression test is included in the supplementary material. The axial and rotational feeds were applied to each die reference point as boundary conditions.

The axial feed and forging frequency were set equal to 1 mm per stroke [22] and 680 hits per minute [23], respectively. The initial and final diameters of the workpiece were assumed to be 15.5 mm and 11.1 mm. Each die moved a distance of 2.2 mm in each stroke; however, since the dies were steep, the amount of diameter reduction in each stroke was dependent on the workpiece axial location under the dies. It was also assumed that supports apply no front-pull and back-push forces at workpiece ends [22].

A constant pressure of 30 MPa was imposed at

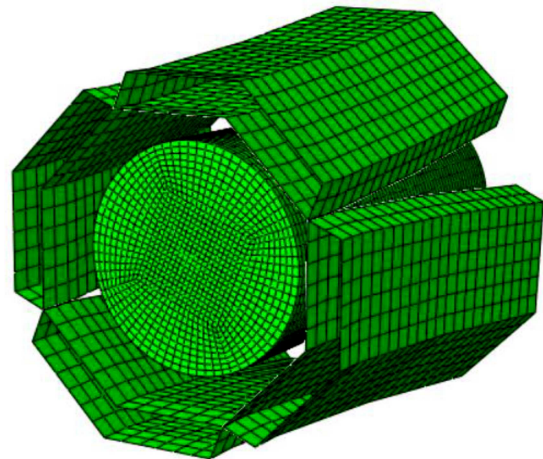
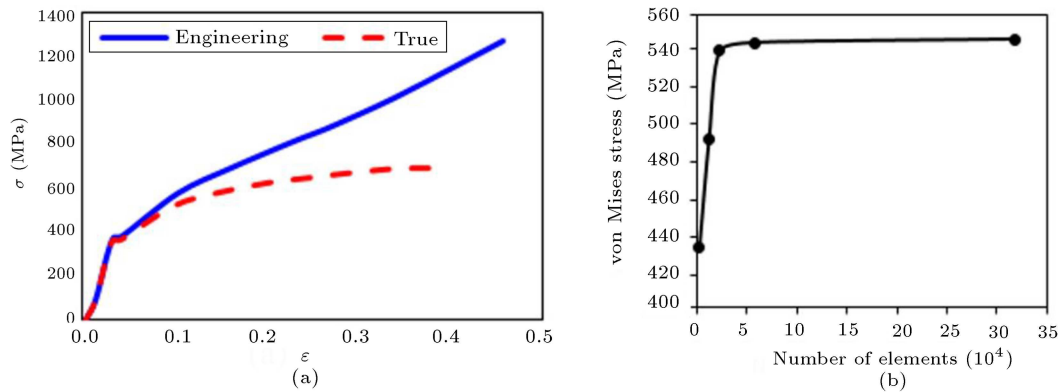
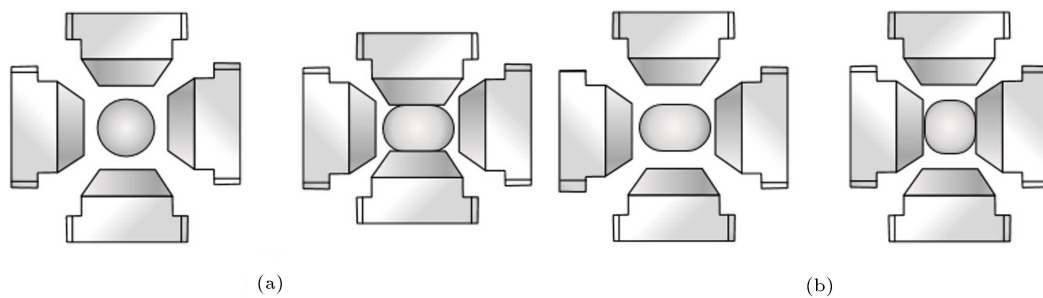


Figure 3. The meshed assembly of the part and dies.



**Figure 4.** (a) The stress-strain curve obtained for the part material; (b) Results of the mesh independence test.



**Figure 5.** (a) The first and (b) the second hit of dies in the radial forging process.

the tube ends to account for back pressure applied by the chuck heads on the tube. This boundary condition was previously proposed in [24].

The Coulomb friction law, expressed as  $\tau = \mu p$ , where  $\tau$  is the frictional shear stress, and  $p$  is the normal stress [1], was used to define the friction at the part-dies interface. The ring compression test was used to measure the coefficient of friction,  $\mu$ . The ring compression test is a standard procedure for determining the friction coefficient in metal forming processes. In this test, a circular ring is axially compressed between two flat dies, which in this paper are the pressure pads of the universal test machine used for performing experimental tests. For a given height reduction, the deformation behavior of the internal diameter of the test specimen can be used to determine the magnitude of the friction coefficient at the die/workpiece interface. Specific calibrated curves can be used to determine the friction coefficient for different values of the inner diameter change and the ratio of compression [25]. In this paper, the value of  $\mu = 0.2$  was obtained by the ring compression test.

## 2.2. Mesh independence test

A mesh independence test has been implemented to ensure an optimum mesh in the FEM. The maximum value of the von Mises stress in the part was compared in meshes with different element densities. The obtained results presented in Figure 4(b) indicate that a

mesh of 58320 elements is a suitable choice. The maximum von Mises stress was observed on the workpiece surface, which has the maximum deformation when in contact with dies.

## 2.3. Verification of the FEM

Normally, numerical models are verified by comparing simulation results with experimental data. Regarding the radial forging process, while numerical and analytical approaches have been widely used to study this process, reliable experimental data are very scarce in the literature. In view of this shortcoming, some authors, e.g., in [26,27], opted to use experimental data reported in a PhD dissertation [28] for the verification of numerical and analytical models of the radial forging process. But these experimental data are very old and, above all, are not reported for the radial forging itself, but for the radial swaging, which bears some similarity to the radial forging process. Consequently, the accuracy of such verifications is disputed.

In order to address this shortcoming, an innovative approach is presented here. To this end, Figure 5(a) illustrates the first forming step in the four-die radial forging process. In this step, two opposite dies hit the lateral surface of the part and then return to their starting position. In the next step, according to Figure 5(b), two other dies lying perpendicular to the path of the first dies hit the part and move back to their initial position.

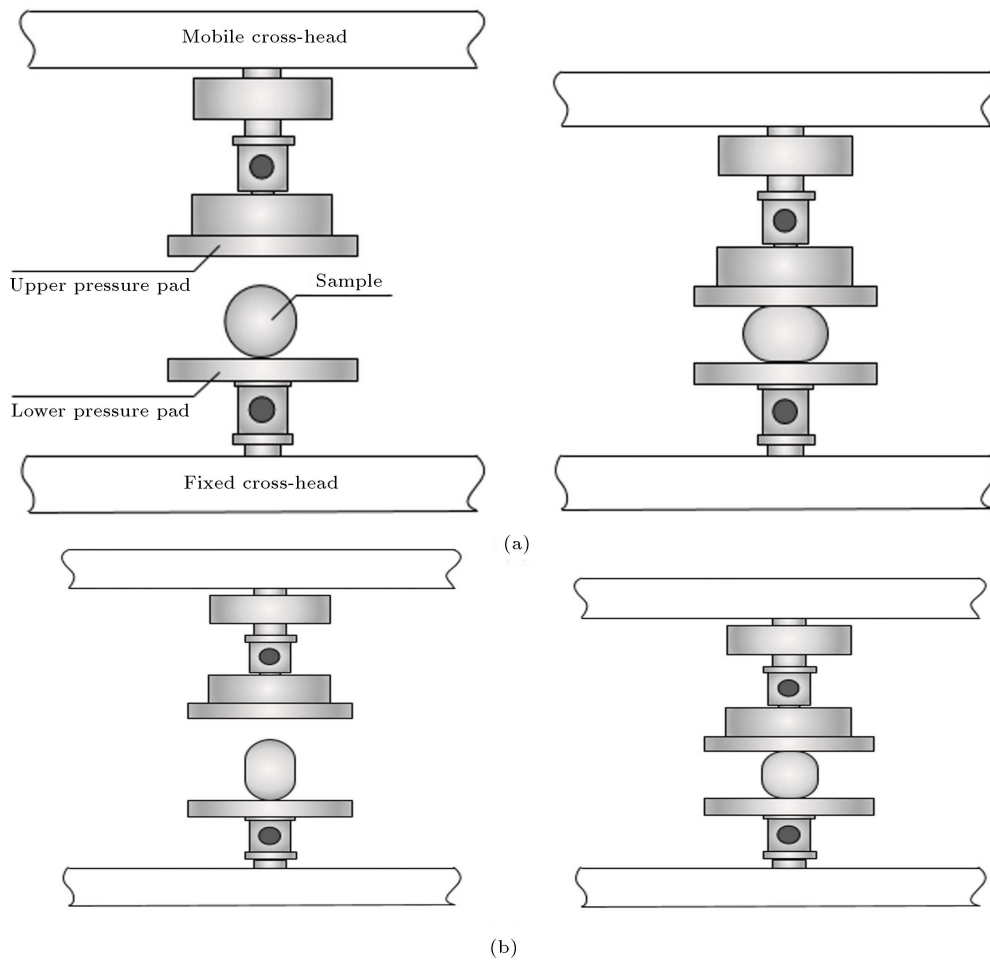


**Figure 6.** (a) The first and (b) the second compression test.

The final product is shaped by multiple hits of dies in combination with part axial and rotational feeds. Therefore, if one only considers the first two hits of dies, the radial forging process is equivalent to a set of two simple compression tests. In the first test shown in Figure 6(a), the lateral surface of a cylindrical sample is flattened by the pressure pads of a universal test machine.

In the second step, the sample is rotated by an angle of  $90^\circ$ , and the first step is repeated, as shown in Figure 6(b).

Since the strain rate effect is negligible at room temperature, the above-described radial forging steps and compression tests are equivalent regardless of the part forming speed. Considering this equivalence, the FEM of the radial forging process can be verified against experimental data taken from the equivalent compression tests.

Figure 7(a) shows, from left to right, the original sample, the sample after performing the first compression test, and the sample after the second compression test. The FEM of the part in the equivalent radial forging process is also shown in Figure 7(b) before and

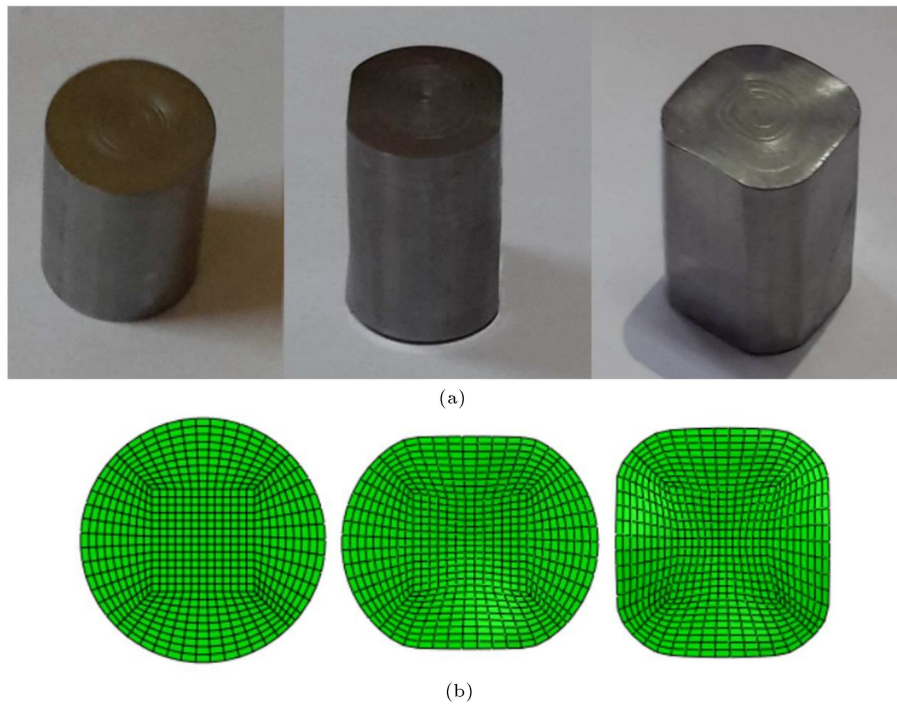
after the first two hits of dies. The sample was made of ST37 steel with a diameter of 15.5 mm and a length of 35 mm. Dies had an inlet angle of  $0^\circ$  and a transverse angle of  $180^\circ$  in the FEM simulation.

Figure 8(a) and (b) compare the forming force obtained in the finite element simulation with corresponding experimental data. The finite element and experimental results are in agreement, as shown in this figure.

### 3. Results and discussion

In this section, the effect of the die transverse angle,  $\beta$ , and the part rotational feed angle,  $\phi$ , is investigated on the final shape and some quality attributes of the radial forging product. The values considered for these parameters are listed in Table 1. A 3D plot of the path on which results are presented is also given in Figure 9(a). The hoop and axial stresses ( $\sigma_\theta$  and  $\sigma_r$ ) are defined according to Figure 9(b).

One of the most important characteristics of all metal forming processes is their capability to form parts as close as possible to the final desired shape. In order



**Figure 7.** (a) The sample shaped in compression tests; (b) The part shaped in the FEM of the equivalent radial forging process.

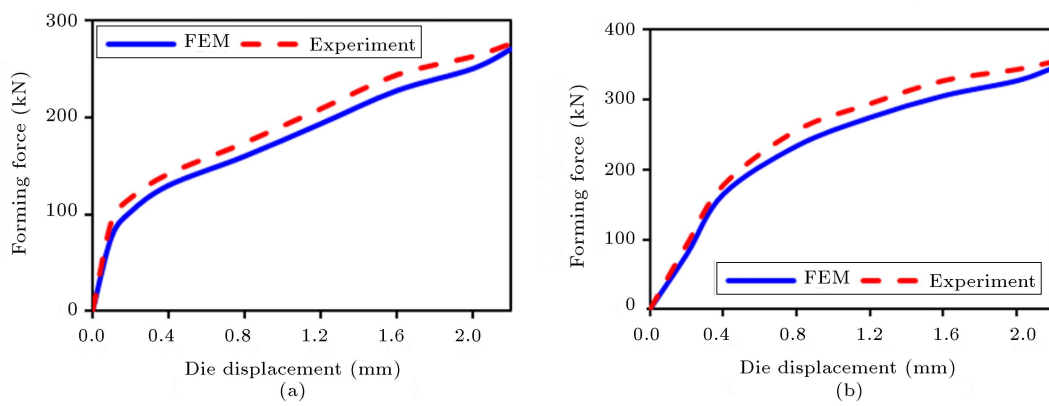


**Figure 8.** The forming force in (a) the first and (b) the second hit of dies.

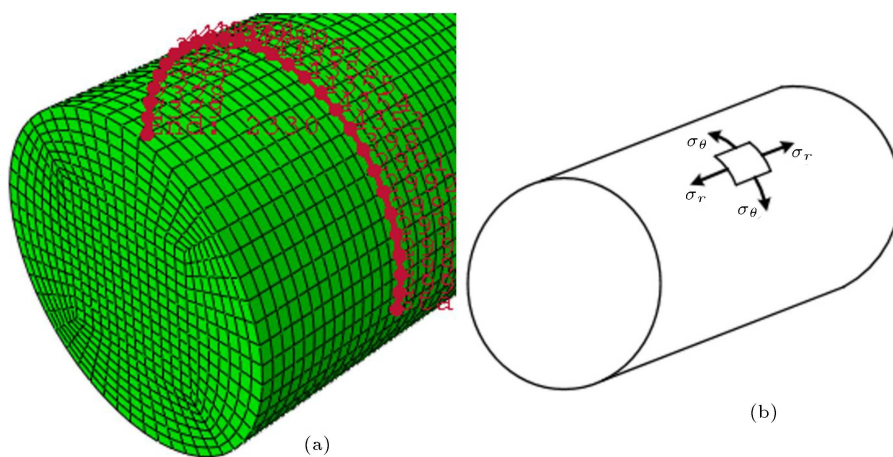


**Figure 9.** (a) A 3D plot of the path on which results are presented; (b) Definition of hoop stress ( $\sigma_\theta$ ) and axial stress ( $\sigma_r$ ).

**Table 1.** The values considered for the die transverse angle  $\beta$  and the part rotational feed angle  $\phi$ .

$\beta$ (deg)	$\phi$ (deg/stroke)
135	11.25
145	22.5
155	45
165	0.19
180	0.37

to measure this characteristic, a new parameter called the percentage of normalized area difference is defined as:

$$A_n = \frac{A_{\text{forged part}} - A_{\text{desired product}}}{A_{\text{desired product}}} \times 100, \quad (2)$$

where  $A_{\text{forged part}}$  and  $A_{\text{desired product}}$  are the cross-sectional area of the forged part and desired product, respectively. The hypothetical cross sections of the desired product and the forged part are presented in Figure 10(a) and (b). If these two cross sections are overprinted, as shown in Figure 10(c),  $A_n$  is equal to the area of the hatched surface divided by the area shown in Figure 10(a) multiplied by 100.

Regarding this definition, a lower value for  $A_n$  means that the part formed closer to its desired shape.

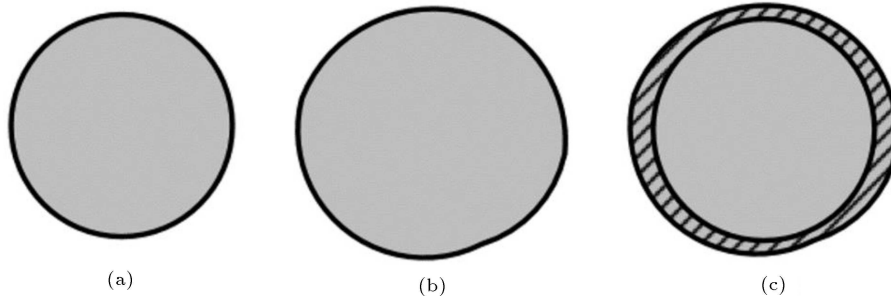


**Figure 10.** Hypothetical cross-section of (a) The desired product, (b) The forged part, and (c) Overprinted cross-sections and hatched area.

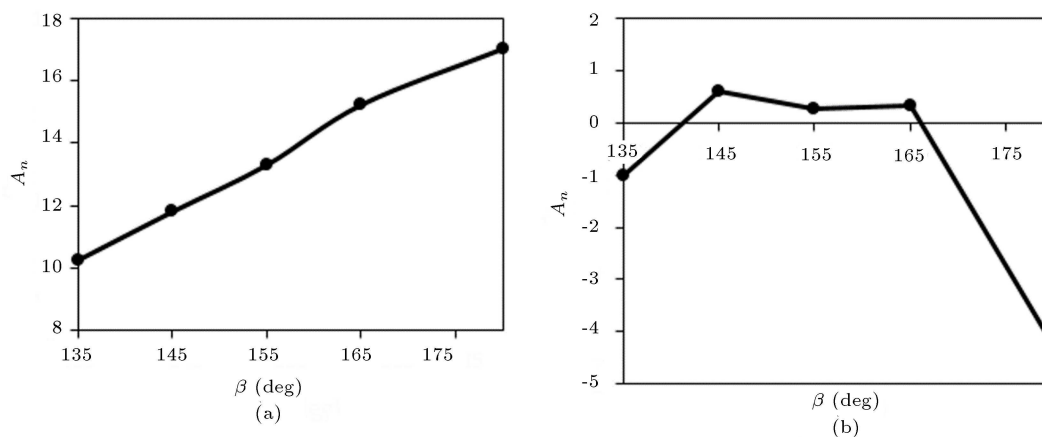


**Figure 11.** Variation of  $A_n$  with  $\beta$  (a) after two hits of dies and (b) after a complete circle rotation of the part.

### 3.1. Effect of the die transverse angle on $A_n$

Figure 11(a) shows the variation of  $A_n$  versus die transverse angle,  $\beta$ , after two hits of dies. According to this figure, in smaller values of  $\beta$ , a lower  $A_n$  is obtained, and the part gets closer to its desired shape. This result seems logical since by reduction of  $\beta$ , the die better encircles the part and creates greater plastic deformation inside it. A view of the deformed part after two hits of dies is shown in Figure 12(a) for  $\beta = 135^\circ$  and  $\beta = 180^\circ$ .

Variation of  $A_n$  with  $\beta$  after a complete circle rotation of the part is shown in Figure 11(b) for the rotational feed angle of  $\phi = 11.25^\circ$ . According to this figure, dies with  $\beta = 155^\circ$  and  $\beta = 165^\circ$  form part closer to its desired shape. The normalized area difference between the forged part and the desired product is about 0.3% or 0.003 in forging with these dies. The die with  $\beta = 180^\circ$  has the worst performance in this respect. A negative value for  $A_n$  in forging by a die with  $\beta = 180^\circ$  may not be expected. This result likely stemmed from the coupled effect of the die transverse angle and rotational feed, and the authors found it very difficult to explain.

$A_n$  is negative for dies with  $\beta = 135^\circ$  and  $\beta = 180^\circ$ . This means that the product cross section becomes smaller than its desired value in forging with

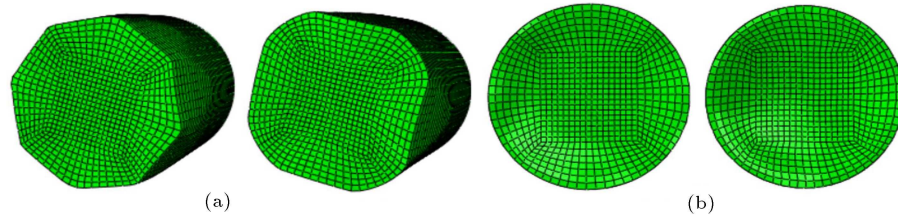


**Figure 12.** (a) Parts shaped by two hits of dies with  $\beta = 135^\circ$  (left) and  $\beta = 180^\circ$  (right) and (b) Part cross-section after a complete rotation for  $\beta = 135^\circ$  (left) and  $\beta = 180^\circ$  (right).

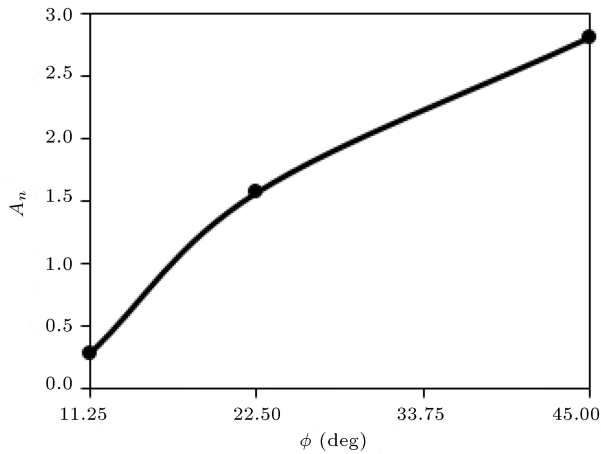


**Figure 13.** Diagram of  $A_n$  variation with rotational feed angle.

these dies. A positive value of  $A_n$  for other transverse angles means that the product cross-section is larger than the desired one for these dies. The deformed cross-section of parts forged by dies with  $\beta = 135^\circ$  and  $\beta = 180^\circ$  is shown in Figure 12(b) for  $\phi = 11.25^\circ$ .

It is worth mentioning that as reported in [29] for rotary feeds of  $45^\circ$ ,  $22.5^\circ$ , and  $11.25^\circ$ , a total rotation angle of  $360^\circ$  (a complete circle rotation) seems to be sufficient for finalizing the strain and RS distribution in the workpiece and obtaining the product desired shape. More discussion about this subject is also present in [29].

### 3.2. Effect of the part rotational feed angle on $A_n$

Variation of the normalized area difference with rotational feed angle is shown in Figure 13. Three rotational feed angles of  $\phi = 11.25^\circ$ ,  $22.5^\circ$ ,  $45^\circ$  are considered for this purpose. According to this figure,  $A_n$  is smaller for smaller values of  $\phi$ , which means that the part gets closer to its desired shape. It can also be seen in Figure 14 that the cross-section of the part forged with  $\phi = 45^\circ$  is not a true circle but a polygon.

### 3.3. Effect of the die transverse angle on the equivalent plastic distribution

The equivalent plastic strain distribution in the part has a profound impact on its mechanical properties. Owing to the strain-hardening effect, the part's me-

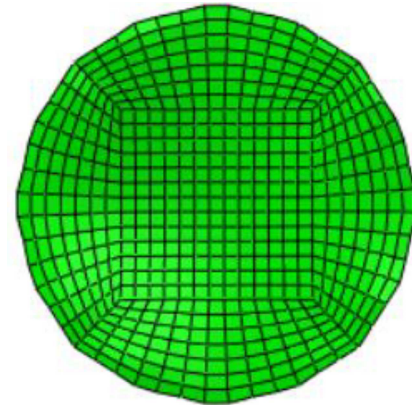


**Figure 14.** Part cross section after a complete rotation for  $\phi = 45^\circ$ .

chanical strength increases with increasing the equivalent plastic strain. Moreover, a more uniform distribution of plastic strain leads to uniformity of mechanical properties, improved RS distribution, and dimensional stability of the process product.

Figure 15(a) shows the distribution of the equivalent plastic strain in the hoop direction of the part surface for dies with different transverse angles. According to this figure, the equivalent plastic strain in the hoop direction is not meaningfully affected by the die transverse angle. Only the transverse angle of  $\beta = 180^\circ$  may be preferred since it makes a larger plastic strain in the part.

The distribution of the equivalent plastic strain in the radial direction of the part is presented in Figure 15(b). As this figure shows, the maximum mean value of the plastic strain distribution occurs in the die with  $\beta = 180^\circ$ , while the maximum uniformity is obtained in forging by a die with  $\beta = 165^\circ$ . It should be noted that the mean value of the plastic strain distribution is 0.34 for  $\beta = 135^\circ$  and 0.38 for  $\beta = 180^\circ$ .

The data shown in Figure 16(a) are for a radial direction that lies at  $\theta = 180^\circ$ . It should be indicated that while the variation of the equivalent plastic strain in other radial directions is different quantitatively, it shows an almost similar qualitative trend (higher strain values in the path start and end points and lower values in the path midpoints) in all radial directions.

The contour of the equivalent plastic strain in



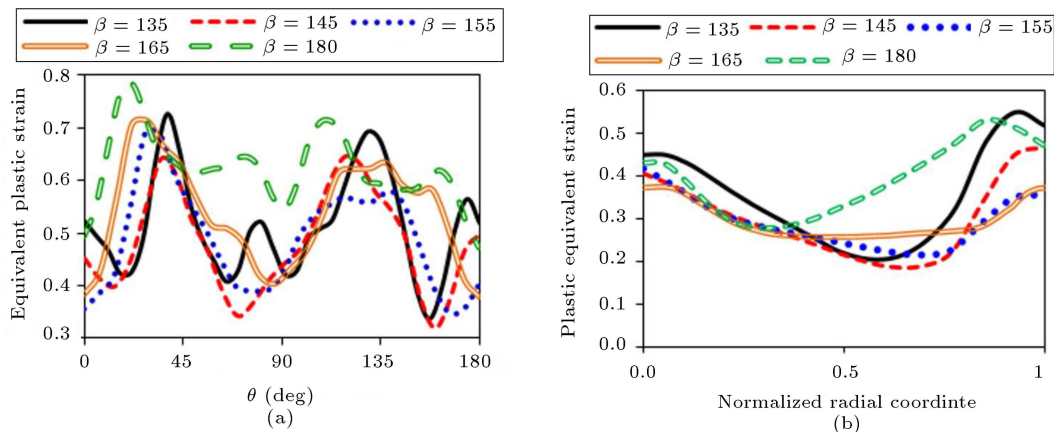


Figure 15. Diagram of equivalent plastic distribution in (a) the hoop direction in the surface and (b) the radial direction.

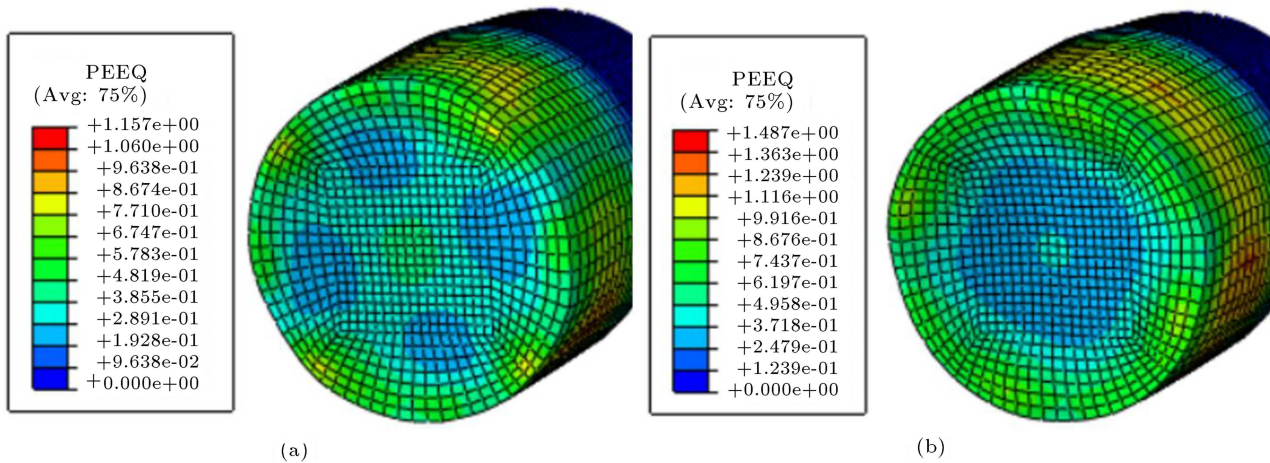


Figure 16. Contour of the equivalent plastic strain in the part forged by a die with (a)  $\beta = 135^\circ$  and (b)  $\beta = 180^\circ$ .

parts forged by dies with  $\beta = 135^\circ$  and  $\beta = 180^\circ$  is shown in Figure 16(a) and (b), respectively.

### 3.4. Effect of the part rotational feed angle on the equivalent plastic strain

Figure 17(a) shows the equivalent plastic strain distribution in the hoop direction of the part surface for different values of the rotational feed angle. According to this figure, a larger plastic strain is made in smaller rotation angles. This may be the consequence of the fact that in smaller rotational feeds, the part withstands more die hits and, therefore, plastic strain before completing full circle rotation.

### 3.5. Effect of the die transverse angle on the RS distribution

RSs directly affect the part life and performance depending on their sign and magnitude. For example, tensile RSs cause fatigue cracks to start and grow and consequently shorten the working life of the part under dynamic loading. Compressive stresses, on the other hand, prevent fatigue cracks from initiating and

developing. Furthermore, RSs affect the dimensional stability of the part and may cause undesired deformation.

Fatigue cracks usually nucleate at the part surface where stresses are highest and where a corrosive environment and geometry changes exist. As a result, stress distribution on the part surface is of prime importance. The die transverse angle effect on the residual von Mises distribution in the hoop direction of the part surface is presented in Figure 17(b). It can be seen in this figure that RSs are more uniform in parts forged by dies with smaller transverse angles. Consequently, higher dimensional stability is expected in these parts.

Figure 18(a) and (b) represent the effect of the die transverse angle on the residual hoop and axial stresses on the part surface for the inlet angle of  $\alpha = 10^\circ$  and feed angle of  $\phi = 11.25^\circ$ . According to this figure, the hoop stress distribution is compressive and very similar for all values of the transverse angle. The axial stress is also compressive at most points of the part surface, and the best distribution is obtained in forging by a die with  $\beta = 165^\circ$ , where compressive

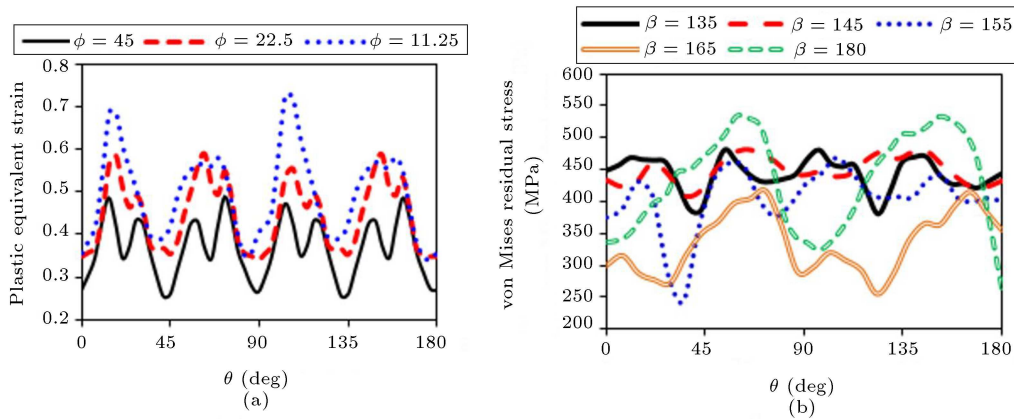


Figure 17. Diagram of (a) the plastic strain and (b) the von Mises residual stress distribution in the part surface.

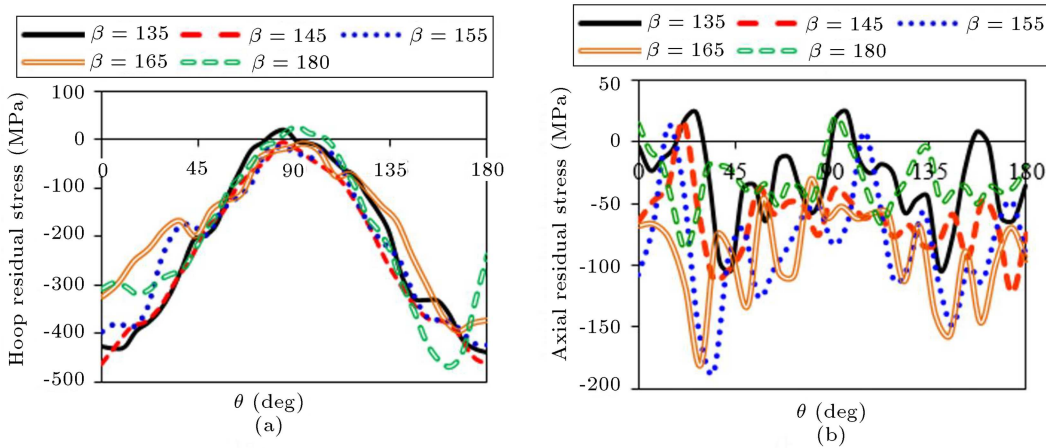


Figure 18. Diagram of (a) the hoop residual stress and (b) the axial residual stress on the part surface.

stresses are created everywhere on the part surface. Compressive hoop and axial stresses developed in most surface points of parts forged by the radial forging process are evidence of the superiority of this process for reducing the part diameter compared with processes such as turning. It can also be seen in Figure 18 that the maximum residual hoop stress occurs at a point with  $\theta = 90^\circ$ . This point lies in the middle of two dies, where the first hits on the part are applied, and consequently, the maximum deformation in the hoop and radial directions is experienced in the first hit. The first hit of dies is important since the maximum deformation of part occurs in this hit.

### 3.6. Effect of the part rotational feed angle on the RS distribution

Diagrams of von Mises, hoop, and axial RS distribution in the part surface are shown in Figures 19 and 20, respectively, for different values of rotational feed angle. According to these figures, the most uniform and the most compressive stress distributions are obtained in  $\phi = 45^\circ$  and  $\phi = 11.25^\circ$ , respectively.

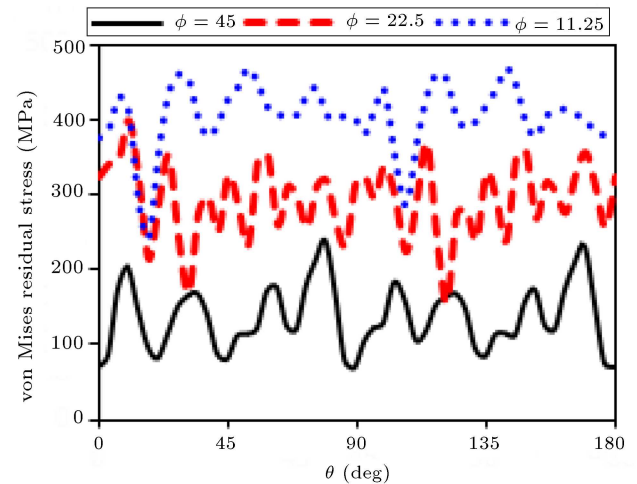
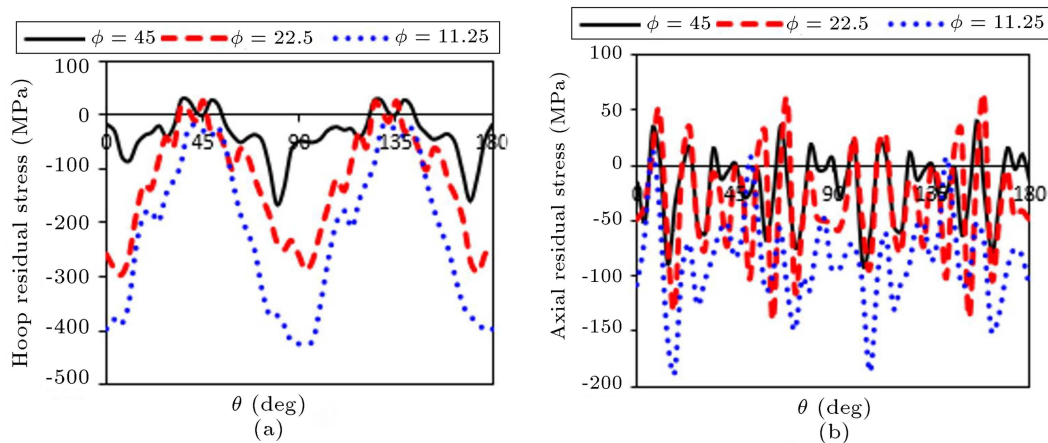


Figure 19. Diagram of the von Mises residual stress in the part surface for different rotational feeds.

## 4. Conclusion

In this paper, the Finite Element Method (FEM) was employed to comprehensively study the effect of the die transverse angle and the part rotational feed angle in



**Figure 20.** Diagram of (a) the hoop residual stress and (b) the axial residual stress in the part surface for different rotational feeds.

the radial forging process for the first time. For this purpose, several steps of the process were simulated by developing a full 3D nonlinear FEM of this process in the ABAQUS software. An innovative experimental approach was also introduced to verify the FEM of the process. The results of this study demonstrated that the dies with transverse angles of  $155^\circ$  and  $165^\circ$  form the part closest to its final shape. Furthermore, the cross-sectional area of the product forged by dies with transverse angles of  $145^\circ$ ,  $155^\circ$ , and  $165^\circ$  is slightly bigger than the desired value, while this area is smaller than the desired value in forging by dies with the transverse angles of  $135^\circ$  and  $180^\circ$ . The die transverse angle has a minor effect on the equivalent plastic strain distribution in the hoop direction. But in the radial direction, the largest plastic strain is created by a transverse angle of  $180^\circ$  and the most uniform plastic strain by a transverse angle of  $135^\circ$ . The von Mises stress is more uniform in parts forged by dies with smaller transverse angles, and increasing the die transverse angle reduces the residual stress uniformity. Reducing the part rotational feed angle leads to the development of higher plastic strain and residual stress on the part surface. Furthermore, it makes residual hoop and axial stresses more compressive.

### Nomenclature

$A_{\text{desired product}}$	Cross-sectional area of the desired product
$A_{\text{forged part}}$	Cross-sectional area of the forged part
$A_n$	Percentage of normalized area difference
$\{U^e\}$	Displacement vector
$\{\ddot{U}^e\}$	Acceleration vector
$F^e$	Mechanical force vector
$K^e$	Finite element stiffness matrix

$M^e$	Finite element mass matrix
$p$	Normal stress
$\beta$	Die transverse angle
$\mu$	Coefficient of friction
$\tau$	Frictional shear stress
$\phi$	Part rotational feed angle

### References

- Afrasiab, H. and Movahhedy, M.R. “Numerical study of the effects of process parameters on tool life in a cold radial forging process”, *Scientia Iranica*, Transaction B, Mechanical Engineering, **21**(2), pp. 339–346 (2014).
- Afrasiab, M., Afrasiab, H., Movahhedy, M.R., et al. “Design of the die profile for the incremental radial forging process”, *Iranian Journal of Science and Technology Transactions of Mechanical Engineering*, **39**(1), pp. 89–100 (2015).
- Li, Y., He, T., and Zeng, Z. “Numerical simulation and experimental study on the tube sinking of a thin-walled copper tube with axially inner micro grooves by radial forging”, *Journal of Materials Processing Technology*, **213**(6), pp. 987–996 (2013).  
<https://doi.org/10.1016/j.jmatprotec.2012.12.002>
- Azari, A., Poursina, M., and Poursina, D. “Radial forging force prediction through MR, ANN, and ANFIS models”, *Neural Computing and Applications*, **25**(3–4), pp. 849–858 (2014).  
<https://doi.org/10.1007/s00521-014-1562-8>
- Sanjari, M., Saidi, P., Karimi Taheri, A., et al. “Determination of strain field and heterogeneity in radial forging of tube using finite element method and microhardness test”, *Materials and Design*, **38**, pp. 147–153 (2012).  
<https://doi.org/10.1016/j.matdes.2012.01.048>
- Sahoo, A.K., Tiwari, M.K., and Mileham, A.R. “Six sigma based approach to optimize radial forging operation variables”, *Journal of Materials Processing Technology*, **202**(1), pp. 125–136 (2008).  
<https://doi.org/10.1016/j.jmatprotec.2007.08.085>

7. Afrasiab, H. “Numerical and analytical approaches for improving die design in the radial forging process of tubes without a mandrel”, *Scientia Iranica, Transactions B: Mechanical Engineering*, **23**(1) pp. 163–173 (2016).
8. Yang, X., Dong, X., and Wu, Y. “An upper bound solution of forging load in cold radial forging process of rectangular cross-section billet”, *Int J Adv Manuf Technol*, **92**, pp. 1–12 (2017).  
<https://doi.org/10.1007/s00170-017-0303-4>
9. Afrasiab, H. “An improved upper bound analysis for study of the void closure behavior in the plane strain extrusion”, *Mechanics Research Communications*, **124**, 103971 (2022).  
<https://doi.org/10.1016/j.mechrescom.2022.103971>
10. Afrasiab, H., Hamzekolaei, M.G., and Hassani, A. “New insight into the radial forging process by an asymptotic-based axisymmetric analysis”, *Applied Mathematical Modelling*, **102**, pp. 811–827 (2022).  
<https://doi.org/10.1016/j.apm.2021.10.030>
11. Darki, S. and Raskatov, E.Y. “Analysis of the hot radial forging process according to the finite element method”, *Int J Adv Manuf Technol*, **110**(3–4), pp. 1061–1070 (2020).  
<https://doi.org/10.1007/s00170-020-05852-3>
12. Wang, X. and Dong, X. “A void evolution model accounting for stress triaxiality, Lode parameter and effective strain for hot metal forming”, *International Journal of Mechanical Sciences*, **168**, 105309 (2020).  
<https://doi.org/10.1016/j.ijmecsci.2019.105309>
13. Yang, Y., Fan, L., and Xu, C. “The microstructure, texture evolution and plasticity anisotropy of 30SiMn2MoVA high strength alloy steel tube processed by cold radial forging”, *Materials Characterization*, **169**, p. 110641 (2020).  
<https://doi.org/10.1016/j.matchar.2020.110641>
14. Xu, W., Mo, J., Zhang, J., et al. “Evolution of residual stress and microstructure during annealing of 30SiMn2MoVA high-strength alloy steel tube processed by cold radial forging”, *J. of Materi Eng and Perform*, **30**(8), pp. 5889–5897 (2021).  
<https://doi.org/10.1007/s11665-021-05834-w>
15. Zuev, L.B., Shlyakhova, G.V., and Barannikova, S.A. “Effect of radial forging on the microstructure and mechanical properties of Ti-based alloys”, *Metals*, **10**(11), p. 1488 (2020).  
<https://doi.org/10.3390/met10111488>
16. Zou, J., Ma, L., Zhu, Y., et al. “Deformation mechanism of ZK60 magnesium bars during radial forging: Mathematical modeling and experimental investigation”, *Materials Characterization*, **179**, p. 111321 (2021).  
<https://doi.org/10.1016/j.matchar.2021.111321>
17. Zou, J., Ma, L., Jia, W., et al. “Microstructural and mechanical response of ZK60 magnesium alloy subjected to radial forging”, *Journal of Materials Science and Technology*, **83**, pp. 228–238 (2021).  
<https://doi.org/10.1016/j.jmst.2020.11.080>
18. Yang, Y., Xu, C., and Fan, L. “Inhomogeneous deformation and texture evolution of 30SiMn2MoVA steel gun barrel processed by radial forging based on cross-scale crystal plasticity finite element method”, *Mat. Res.*, **25** pp. 48–56 (2022).  
<https://doi.org/10.1590/1980-5373-MR-2022-0115>
19. Makiyama, T. “Effects of rotational feed emulating four-die radial forging on forged shape in mandrel-less incremental forging of thick circular tube”, *Presentations and Videos to 16th International Conference on Computational Plasticity (COMPLAS 2021)*, IS02-Applications of Computational Methods to Product and Process Design for Industry (2022).  
<https://doi.org/10.23967/complas.2021.022>
20. Darki, S., and Raskatov, E.Y. “Development of an analysis method for radial forging parameters based on hardness criterion”, *Journal of Mechanical Engineering, New Material and Technology Institute Ural Federal University*, **20**(1), pp. 149–167 (2023).  
<https://doi.org/10.24191/jmeche.v20i1.21084>
21. Mackey, B.T., Siegmund, T., and Sangid, M. “Simulating the evolution of non-metallic inclusions during the forging process”, *Journal of Manufacturing Science and Engineering*, **145**(7), pp. 1–48 (2023).  
<https://doi.org/10.1115/1.4057026>
22. Ghaei, A., Karimi Taheri, A., and Movahhedy, M.R. “A new upper bound solution for analysis of the radial forging process”, *International Journal of Mechanical Sciences*, **48**(11), pp. 1264–1272 (2006).  
<https://doi.org/10.1016/j.ijmecsci.2006.06.002>
23. Fan, L., Wang, Z., and Wang, H. “3D finite element modeling and analysis of radial forging processes”, *Journal of Manufacturing Processes*, **16**(2), pp. 329–334 (2014).  
<https://doi.org/10.1016/j.jmapro.2014.01.005>
24. Ghaei, A. and Movahhedy, M.R. “Die design for the radial forging process using 3D FEM”, *Journal of Materials Processing Technology*, **182**(1), pp. 534–539 (2007).  
<https://doi.org/10.1016/j.jmatprotec.2006.09.013>
25. Sofuoglu, H., Gedikli, H., and Rasty, J. “Determination of friction coefficient by employing the ring compression test”, *J. Eng. Mater. Technol*, **123**(3), pp. 338–348 (2000).  
<https://doi.org/10.1115/1.1369601>
26. Ghaei, A., Movahhedy, M.R., and Karimi Taheri, A. “Finite element modelling simulation of radial forging of tubes without mandrel”, *Materials and Design*, **29**(4), pp. 867–872 (2008).  
<https://doi.org/10.1016/j.matdes.2007.03.013>
27. Alaei, E., Afrasiab, H., and Dardel, M. “Analytical and numerical fluid-structure interaction study of a microscale piezoelectric wind energy harvester”, *Wind Energy*, **23**(6), pp. 1444–1460 (2020).
28. Uhlig, A. “Investigation of the motions and the forces in radial swaging”, *Technical University Hannover* (1964).  
<https://doi.org/10.1002/we.2502>

29. Afrasiab, H. and Movahhedy, M.R. “Numerical study of the workpiece rotation effect on the strain and residual stress distribution in the cold radial forging process”, pp. 785–792 (2010).  
<https://doi.org/10.1115/ESDA2010-25122>

### Biographies

**Mozhdeh Fattahpoor Roushan** received her BSc and MSc degrees, both in Mechanical Engineering, from Babol Noshirvani University of Technology, Iran, in 2014 and 2016, respectively. She is currently a PhD student at the same university. Her main research interests are finite element simulation and modeling of metal forming processes.

**Hamed Afrasiab** received his BSc, MSc, and PhD degrees, all in Mechanical Engineering, from Sharif

University of Technology, Iran, in 2004, 2006, and 2011, respectively. He is currently an Associate Professor at the department of Mechanical Engineering, Babol University of Technology, Iran. His main research interests are mechanics of fuel cell components, finite element method, composite materials, sandwich structures, and modeling of metal forming processes.

**Ramazan-Ali Jafari Talookolaei** is currently an Assistant Professor at the Department of Mechanical Engineering, Babol Noshirvani University of Technology, Iran. He received his BSc in Mechanical Engineering from Shahrood University of Technology in 2002 and his MSc and PhD degrees in Mechanical Engineering from Sharif University of Technology in 2004 and 2013, respectively. His main research interests are laminated composite structures, finite element method, vibrations, and damaged structures.